Hindawi
Advances in Civil Engineering
Volume 2020, Article ID 3193012, 17 pages
https://doi.org/10.1155/2020/3193012

Research Article

Influence of Multiple Factors on the Explosion Characteristics of Flammable Gases in Municipal Sewage Pipelines

Pengfei Lv, Jiaxu Zhang, Lei Pang, Kai Yang, and Siheng Sun

Safety Engineering College, Beijing Institute of Petrochemical Technology, Beijing 102617, China

Correspondence should be addressed to Lei Pang; pang@bipt.edu.cn

Received 19 November 2019; Revised 25 June 2020; Accepted 30 August 2020; Published 8 September 2020

Academic Editor: Bingxiang Yuan

Using the hydrodynamic software Fluidyn, a numerical model comprising a top-sealed vertical inspection well and a horizontal well with openings at both ends was built based on symmetry, to study the explosion propagation of flammable gases in typical municipal sewage pipelines. The vertical well had a diameter of 0.7 m and different depths (2 m, 4 m, and 6 m), and the horizontal well had a diameter of 0.8 m and a length of 20 m at both sides. The effects of different ignition positions, well depths, and gas compositions and concentrations on the explosion characteristics and rules governing the propagation of flammable gases in a municipal sewage pipeline were investigated. The findings suggest that different ignition positions (at the top, middle, and bottom of the inspection well) did not lead to a significant difference between peak explosion pressure and temperatures but had a substantial influence on the propagation velocity of the explosion flame near the corner of the junction between the vertical inspection well and the horizontal well. Different inspection well depths had no significant impact on the peak explosion pressure or temperature but had a substantial effect on the propagation velocity of the explosion flame at the bottom of the well. Compared with a methane (CH_4) explosion at a concentration of 6%, the peak explosion pressure, peak explosion temperature, and flame propagation velocity of a CH_4 and oil-gas mixture at a concentration ratio of 6% : 1% were found to be significantly higher. With increasing oil-gas concentrations (2%, 4%, and 6%), the peak pressure, temperature, and flame propagation velocity continued to decrease. The findings of this study can help prevent explosion accidents in municipal sewage pipelines and provide a reference to support the establishment of related standards.

1. Introduction

As an essential part of urban public infrastructure, municipal sewage pipelines are highly vulnerable to gas explosion accidents leading to heavy casualties and property losses because flammable gases often accumulate due to the massive scale of the sewer system, its numerous branches, and its airtightness. For example, a volatile oil-gas mixture accumulated within a closed municipal sewage conduit and exploded because of a spark during the Sinopec Donghuang underground oil pipeline leakage and explosion accident in Qingdao, Shandong Province, China, on November 22, 2013. This accident resulted in 62 deaths, 136 injuries, and a direct economic loss of nearly RMB 752 million. In the underground gas pipeline leakage and explosion accident in Kaohsiung, Taiwan, China, on August 1, 2014, the leaked gas spread along a drainage box culvert and exploded upon heat exposure, killing 30 people and injuring 310. Therefore, it is essential to study the prevention and control of gas explosion disasters in municipal sewage pipelines.

A series of studies on gas explosion within confined spaces such as municipal sewage pipelines has been performed. Considering that a large number of structures with complex geometry, such as L and T shapes, exist within sewage pipelines, a comparative experiment was conducted by Li et al. [1] to study the influence of T-shaped branch pipes on the overpressure and flame propagation velocity of an oil-gas explosion within the airtight pipeline. The results indicated that the maximum overpressure of a T-shaped pipe increased with the distance of ignition, and oscillation was observed. Furthermore, the T-shaped branch structure placed within the sealed pipeline increased the explosion

overpressure and flame propagation velocity. Wang et al. [2] studied the influence of a T-shaped bifurcation tube on flame propagation and gas explosion by using the schlieren system and a high-speed camera. The propagation of gas explosion within a bent pipeline was investigated in an experimental study by Zhai et al. [3]; the findings suggested that the explosion and flame propagation velocity rose sharply at the bend due to the interaction between the pressure wave and flame. According to Blanchard et al. [4], the explosion overpressure and flame propagation velocity of a CH_4-oxygen (O_2) mixture were increased by the 90°-bent pipe. Xiao et al. [5, 6] proposed that the flame shape in a 90°-bent tube had four transmission processes, and its influence on the flame structure was mainly in the pipe behind the elbow. Yang et al. [7] studied the propagation law of the detonation wave of propane-air premixed gas in a vertical "Z-" type pipe with two 90° elbows. It was found that the "Z-" type pipe attenuated the unsteady detonation wave, and its influence depended on the wave's propagation velocity. Five branch pipes were designed by Zhang et al. [8] to study the influence of the pipe structure on the explosion characteristics of a gasoline-air mixture, revealing that the maximum explosion pressure, rate of overpressure increase, and explosion index were increased by branch pipes. In addition, the maximum flame propagation velocity demonstrated an increasing-decreasing trend with an increasing number of branch pipes. Pang et al. [9] performed explosion experiments in tunnels with different turning angles and obtained the distribution law of the high-temperature flow field before and after the turns.

Ignition position influences the explosion characteristics of flammable gases. In an experimental study of the influence of the ignition position within a cylindrical depressurisation vessel upon the peak explosion overpressure, when a CH_4-O_2 mixture was ignited in the middle, Chao et al. [10] observed a "double peak" phenomenon. In a study by Guo et al. [11], the influence of ignition position on the explosion and depressurisation of a hydrogen-air mixture within a vessel with a small length-to-diameter ratio was examined. The highest internal explosion overpressure occurred when the mixture was ignited at the middle, and the highest external explosion overpressure occurred when it was ignited at the opening. In addition, the flames formed by the ignition at the middle and the opening were longer than by the ignition at the bottom. The rules governing the transmission of pressure waves in a pipeline gas explosion were studied [12], revealing that the maximum value of the pressure wave initially decreased near the explosion point, then rose to a peak, and then decreased gradually. Furthermore, obstacles also significantly enhanced the overpressure, overpressure rise rate, and flame speeds. Notably, the obstruction geometry and blockage ratio had significant effects on the explosion characteristics of gas mixtures in closed pipes [13]. Regarding other factors influencing explosion characteristics, an experimental investigation of the interaction between propagating premixed flames with various solid obstructing bodies was performed by Masri et al. [14] to quantify the role of turbulence in flame acceleration and structure. Obstructions with circular, triangular, and square cross sections were studied, and the results showed that the obstruction with the rectangular cross section caused the highest acceleration, while the lowest was associated with the circular cross section. The blockage ratio significantly affected the flame acceleration in the rectangular cross section case, while the circular and triangular cross section obstacles demonstrated less influence. In another study by Razus et al. [15], the pressure-time evolution during the deflagration of gaseous propylene-air mixtures in the presence of their exhaust gas was experimentally investigated in a spherical vessel, over an extended range of equivalence ratios, at room temperature and initial pressures of 0.3–1.0 bar. The results showed that the exhaust gas had a significant inerting effect on the flammable fuel-air mixtures and could be considered an inexpensive, ready-to-use diluent for the mitigation of fuel-air explosions.

Nie et al. [16] considered the influence of a foam-ceramic material on gas explosion pressure and flame propagation properties and found that the pressure variation depended on the propagation velocity and the position of the flaming plane during a gas explosion. The laminar burning velocity during a gas explosion was analysed by Huzayyin et al. [17] based on the relationship between the pressure and flaming plane. An experimental study on the flame propagation velocity within a small-scale square-bent pipe by Sato et al. [18] revealed that the flame propagation velocity increased significantly when passing through a bend, decreased slightly afterwards, and accelerated upon leaving the end of the pipe. By conducting a gas explosion experiment using a semi-closed pipe, Fairweather et al. [19] found that the explosion flame propagated in a laminar manner; significant overpressure occurred due to the fast turbulent combustion formed at the end of the explosion. According to an experimental study by Valiev [20], the increase in flame propagation velocity primarily depended on the geometrical shape of the pipe; a pipe with a smooth wall surface and a symmetrical structure was more conducive to flame propagation from the closed end to the outside. Thomas et al. [21] used an unobstructed pipe to study the flame acceleration process, which was divided into three distinct phases: an initial establishment phase, a second rapid acceleration phase, and a final transition to detonation phase.

Researchers have conducted relevant studies on the explosion propagation characteristics of combustible gas in pipelines with complex structures. However, the primary consideration has been the influence of the pipeline structure, while the composition and concentration of combustible gas are relatively less studied. The structure and size of the municipal sewage pipe network, ambient temperature and humidity, ignition position, and gas composition and concentration, among other factors, will affect a gas explosion in a municipal sewage pipe network. Previous studies have failed to fully account for the characteristics of the municipal sewage pipeline and are inadequate in revealing the explosion characteristics of flammable gases and the evolution and propagation of explosion disasters. This

lack of available research has restricted the identification of the mechanisms of explosion disasters within municipal sewage pipelines and the development of techniques to prevent and control them. To this end, the flammable gas explosion properties within a municipal sewage pipeline, including pressure, temperature, and flame propagation velocity, were investigated by considering factors including ignition position, inspection well depths, and gas compositions and concentrations. The results provide a reference for the prevention of explosion accidents in municipal sewage pipelines and the development of safety management standards.

2. Numerical Model

2.1. Numerical Method. The three-dimensional (3D) hydrodynamic simulation software Fluidyn-MP was used to investigate the influence of multiple factors on the explosion characteristics of flammable gases within a municipal sewage pipeline. Developed by Fluidyn (France), Fluidyn-MP is a multiphysics simulation software with numerous functions, which is dedicated to the simulation of explosion, deflagration, and detonation in 3D confined, semiconfined, and open spaces. It is also able to accurately simulate the 3D flow of fluid and coupled physical phenomena. With this software, a flammable gas explosion can be assumed to be a single-step irreversible chemical reaction. The dynamic gas behaviour during a gas explosion can be determined by using the finite volume method to solve a series of equation sets, such as the equations for the conservation of mass, momentum, and energy. Furthermore, the turbulent behaviour during a gas explosion can be simulated using the k-ε model. The equations used in this study are as follows:

$$\frac{\partial \rho}{\partial t} + \nabla \cdot (\rho U) = S_p, \tag{1}$$

$$\frac{\partial (\rho U)}{\partial t} + \nabla \cdot (\rho U U) = \nabla \cdot \tau - \nabla p + S_u, \tag{2}$$

$$C_p \left[\frac{\partial (\rho T)}{\partial t} + \nabla \cdot (\rho U T) \right] = -\nabla \cdot q + \left[\frac{\partial \rho}{\partial t} + U \cdot \nabla p \right] + \tau : \nabla U + S_T. \tag{3}$$

Equations (1)–(3) are the equations for the conservation of mass, momentum, and energy, respectively. ρ, U, S_p, τ, S_u, C_p, T, q, p, and S_T are the density, velocity vector, the source term of the equation of continuity, viscous stress tensor, the source term of the momentum equation, the specific heat at constant pressure, temperature, heat flux vector, pressure, and the source term of the temperature equation, respectively:

$$\begin{aligned} \frac{\partial (\rho k)}{\partial t} + \nabla \cdot (\rho U k) &= \nabla \cdot \left(\mu_l + \frac{\mu_t}{\sigma_k} \right) \nabla k \\ &\quad + P_k + P_b - \rho \varepsilon - \frac{2}{3} \rho k \nabla \cdot U + S_k^v, \\ \frac{\partial (\rho \varepsilon)}{\partial t} + \nabla \cdot (\rho U \varepsilon) &= \nabla \cdot \left(\mu_l + \frac{\mu_t}{\sigma_\varepsilon} \right) \nabla \varepsilon \\ &\quad + \frac{\varepsilon}{k} \left[C_{\varepsilon 1} \left(P_k + P_b \right) - C_{\varepsilon 2} \rho \varepsilon \right] \\ &\quad - \left(\frac{2}{3} C_{\varepsilon 1} - C_{\varepsilon 3} \right) \rho \varepsilon \nabla \cdot U + S_\varepsilon^v, \end{aligned} \tag{4}$$

where μ_l and μ_t are viscosities; P_k is the mechanical production rate of k; P_b is buoyancy production rate of k; S_k^v and S_ε^v are the source terms due to vegetation canopy; and σ_k, σ_ε, $C_{\varepsilon 1}$, $C_{\varepsilon 2}$, and $C_{\varepsilon 3}$ are the constants.

An improved BML combustion model was applied. The reaction rate ω complied with

$$\omega = C_1 \overline{\rho} \Gamma_k \frac{\varepsilon}{k} (1 + \tau) \frac{\overline{c} (1 - \overline{c})}{(1 + \tau \overline{c})}, \tag{5}$$

where C_1, $\overline{\rho}$, ρ_R, T_b, T_u, $\overline{c}$, and Γ_k are the empirical coefficient, normalized density, reactant density, the temperature of combustion product, the temperature of unburned reactant, overall progress variable, and normalized tensile rate, respectively:

$$\begin{aligned} \overline{\rho} &= \frac{\rho_R}{(1 + \tau \overline{c})}, \\ \tau &= \frac{T_b}{(T_u - 1)}. \end{aligned} \tag{6}$$

The conservation equation of each component can be denoted as

$$\frac{\partial (\rho y_m)}{\partial t} + \nabla \cdot (\rho U y_m) = \nabla \cdot D_m \nabla (y_m) + S_m, \tag{7}$$

where y_m, D_m, and S_m are the mass fraction of component m, effective diffusion coefficient of component m, and the source term of the conservation equation of component m, respectively.

2.2. Experimental Verification of the Numerical Model. The numerical simulation results were compared with previously obtained experimental results [22] to verify the

effectiveness of the proposed numerical method. In the experiment, a CH_4-air mixture explosion was simulated within a pipeline, as shown in Figure 1. This pipeline consisted of five sections of short round pipes numbered as 1, 2, 3, 4, and 5; Pipe 1 was 0.4975 m long, and Pipes 2–5 were 0.995 m long. The pipes were connected by using circular flanges to form a straight pipe with a length, internal diameter, and wall thickness, of 4.4775 m, 0.199 m, and 0.01 m, respectively, and had a maximum compression strength of 5 MPa. The left end of the pipeline was open, the right end was sealed as the ignition end, and there was a layer of plastic film between Pipes 2 and 3. Pipes 1 and 2 were filled with CH_4 and kept upright to ensure the thorough mixing of the air and CH_4. The volume concentration of CH_4 within the pipes was approximately 10.2%. Five pressure sensors were mounted along the pipeline at the positions where the ratios between the distance to the ignition end and the inner pipe diameter (L/D) were 1.25, 5, 10, 15, and 20.

The numerical model was built based on the experimental conditions, and the pipeline size and test points were consistent with those in the experiment. CH_4 was filled into the pipeline until its concentration reached 10.2%. The pipe wall was assumed to be adiabatic and smooth, with the initial pressure and temperature set to 0.1 MPa and 298 K, respectively. As shown in Figure 2, the numerical simulation results were compared with the experimental results.

It can be seen from Figure 2 that the peak overpressure curves obtained from the numerical simulation closely matched with those obtained from the experiment and showed an increasing-decreasing trend with increasing L/D. Specifically, the mean absolute and relative errors were 1.5 kPa and 7.9%, respectively, and they were attributed to the roughness and wall heat dissipation of the experimental pipeline, the accuracy and sensitivity of the pressure sensors, the precision of the numerical simulation grid, and other unknown reasons. Based on the comparative verification between the numerical simulation and experiment, it was reasonable to use the proposed numerical method.

2.3. Research Scheme. Municipal sewage pipelines are widely distributed under urban roads and usually consist of vertical inspection wells and horizontal wells. An inspection well is approximately 0.7 m in diameter and 2–6 m in depth; the distance between two inspection wells is approximately 50 m; and the diameter of the horizontal well is typically 0.4–1.0 m. In most cases, flammable gases, such as CH_4 and oil-gas (C_8H_{18}), accumulate in the sewage pipeline, which thus becomes highly vulnerable to an explosion during a fire. For convenient analysis, the municipal sewage pipeline was simplified during the numerical simulation. A numerical model comprising a top-sealed vertical inspection well with a diameter of 0.7 m and different depths (2 m, 4 m, and 6 m) and a horizontal well with a diameter of 0.8 m, a length of 20 m at each side, and openings at both ends was built based on symmetry (Figure 3). Test points were set within the model to monitor the data such as explosion pressure and temperature. Specifically, test points 1–11 were set within the horizontal well at an interval of 2 m; test point 12 was placed at the junction of the centrelines of the horizontal well and the inspection well; test points 13–21 were placed within the vertical inspection well at an interval of 0.5 m for well depths of 1 m, 2 m, and 4 m when the well depth was 6 m.

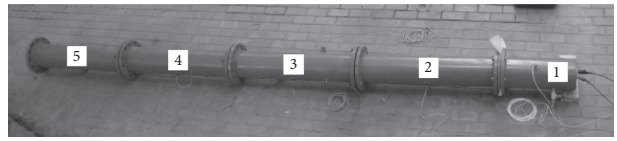

Figure 1: Experimental pipeline [22].

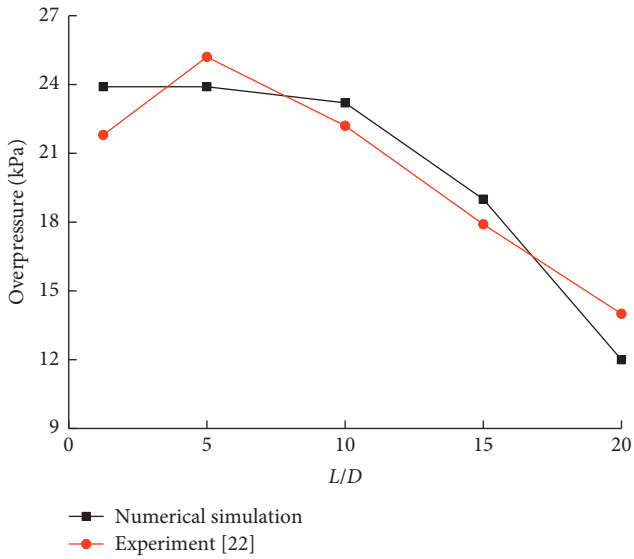

Figure 2: Comparison curve of numerical simulation and experimental peak overpressure.

Nine simulation schemes (Table 1) were designed to investigate the influence of different ignition positions, inspection well depths, gas compositions, and concentrations on the explosion and propagation of flammable gases within a municipal sewage pipeline. Due to the uneven distribution of combustible gas composition and concentration in a sewage pipe network, only representative CH_4 and C_8H_{18} were selected as the gas components for simulation. The inspection well depths were 2 m, 4 m, and 6 m; gas compositions and concentrations were 6% CH_4, 2% C_8H_{18}, 4% C_8H_{18}, 6% C_8H_{18}, and 6% CH_4 + 1% C_8H_{18}; and ignition positions were at the top, middle, and bottom of the inspection well. During the simulation, both the inspection well and the horizontal well were filled with gases. The boundary condition was assumed to be adiabatic and smooth; the initial pressure and temperature were set to 101.325 kPa and 298 K, respectively.

3. Results and Discussion

3.1. Influence of the Ignition Position. As shown in Table 1, the inspection well depth was set to 4 m; ignition positions were at the top, middle, and bottom of the inspection well, and the corresponding positions were test points 21, 17 and 13, respectively. The inspection well was sealed at the top,

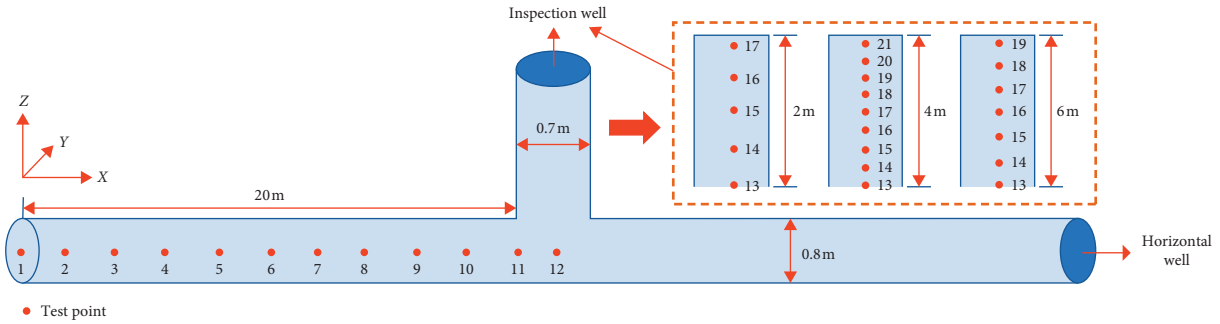

Figure 3: Model schematic diagram.

Table 1: Simulation schemes.

Factors	Inspection well depth (m)	Gas concentration and composition	Ignition position	Ignition position test points
Influence of ignition position	4	6% CH_4	Top Center Bottom	Test point 21 Test point 17 Test point 13
Influence of inspection well depth	2 4 6	6% CH_4	Center	Test point 15 Test point 17 Test point 16
Influence of gas composition	4	6% CH_4 6% CH_4 + 1% C_8H_{18}	Center	Test point 17
Influence of gas concentration	4	2% C_8H_{18} 4% C_8H_{18} 6% C_8H_{18}	Center	Test point 17

and both ends of the horizontal well were open during the simulation. The inspection well and the horizontal well were filled with 6% CH_4.

3.1.1. Influence of the Ignition Position on the Explosion Pressure. Observations were made in test points 1, 6, 12, and 17, located at the left end of the horizontal well, the middle of the horizontal well, the junction of the horizontal well and the vertical inspection well, and the middle of the inspection well, respectively. Figure 4 shows the pressure-time variation curves for various test points at the ignition positions at the top, middle, and bottom of the inspection well.

Figure 4(a) shows that the test points demonstrated similar pressure-time variation trends when the ignition position was at the top of the inspection well. Over time, the pressure first increased, then decreased, and repeatedly oscillated thereafter. The peak pressure and oscillation amplitudes differed significantly between the different test points; they were the greatest at test points 12 and 17, followed by test points 6 and 1. The peak pressure and oscillation amplitudes decreased as the distance to the ignition position increased (i.e., the distance to the left end of the horizontal well decreased). The pressure oscillation was maintained at approximately 101.325 kPa. The analysis shows that when methane was ignited, it underwent accelerated combustion expansion and released tremendous energy, resulting in a pressure rise and peak value. The methane combustion ultimately resulted in pressure decay. The openings at both ends of the horizontal well provided explosion depressurisation with channels. The explosion pressure decreased as proximity to the pipe end increased, which manifested as a low peak pressure and rapid decrease of the explosion pressure after the peak, due to the effect of the end depressurisation. In addition, the explosion wave that spread from the end resulted in a higher negative pressure within the horizontal and inspection wells. The external air was pulled into the end of the horizontal well, and the gas in the horizontal well caused pressure oscillations due to this piston effect. Therefore, some test points experienced strong Helmholtz oscillations; this is corroborated by the experimental results obtained by Hisken et al. [23] and Wan et al. [24]. Figures 4(b) and 4(c) suggest that when the ignition positions were at the middle and the bottom of the inspection well, the pressure-time variations were similar to the case in Figure 4(a). Figure 5 provides the peak pressure variation curves that were developed based on the simulation results for various test points when the ignition positions were at the top, middle, and bottom of the inspection well.

As shown in Figure 5, the peak pressure variation curves exhibited consistent trends for the ignition positions at the top, middle, and bottom of the inspection well and presented a marked segmentation at test point 8. Specifically, the peak pressure from test point 8 to 1 decreased, dropping to the minimum at test point 1 (at the left end of the horizontal well). The three peak pressure variation curves overlapped each other. From test point 9 to 21, the peak pressure remained stable and was maintained at approximately

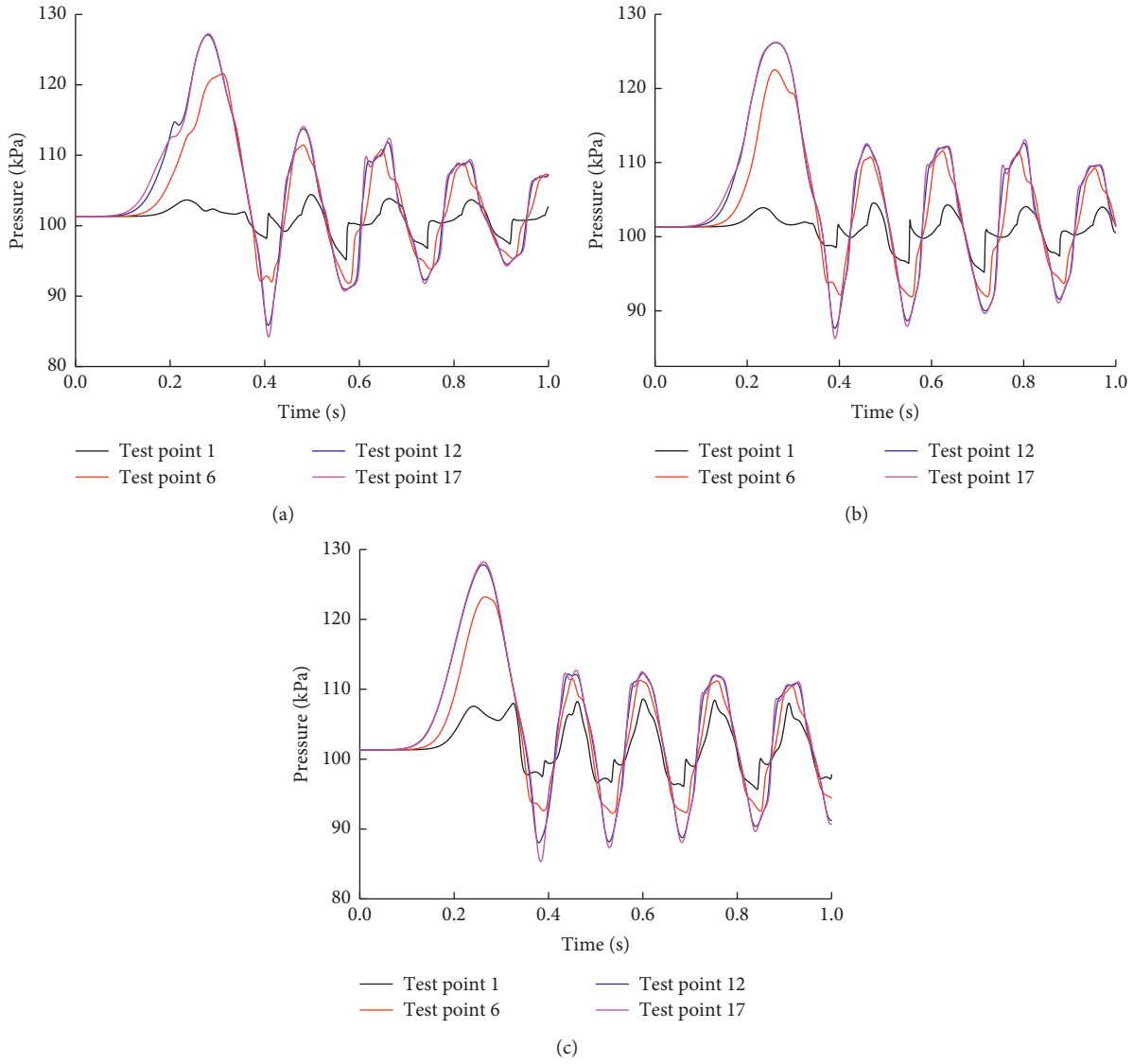

Figure 4: Curves of pressure vs. time under different ignition positions. (a) Top ignition. (b) Center ignition. (c) Bottom ignition.

128 kPa, 127 kPa, and 129 kPa when the ignition positions were at the top, middle, and bottom of the inspection well, respectively. Different ignition positions did not result in significant differences in peak pressure, and, for all the ignition positions, the pressure increased gradually as the explosion reaction progressed. Because the sealed top of the inspection well created a relatively confined space (test points 9–21), the probability of collision between the combustible gas molecules increased, thus increasing the degree of the chemical reaction and maintaining a high peak explosion pressure. Due to the end depressurisation effect, during the explosion, intense pressure was released at the left end of the horizontal well and the surrounding area (test points 1–9). Additionally, the amount of the reactants decreased due to the leakage of unburned gases from both ends, leading to different degrees of peak pressure attenuation and explaining the segmentation of the peak pressure curves.

3.1.2. Influence of the Ignition Position on the Explosion Temperature. Through observation of the area from the left end of the horizontal well to the ignition position, the peak explosion temperature variation curves were obtained for ignition positions at the top, middle, and bottom of the inspection well (Figure 6).

Figure 6 shows that near the ignition position, high explosion temperatures were maintained, and the peak temperature curves varied consistently when the ignition positions were at the top, middle, and bottom of the inspection well, peaking at 1713 K, 1710 K, and 1705 K, respectively. According to the analysis, the methane reacted quickly and released a large amount of heat within a short time after ignition, and the temperature rose rapidly to the peak. The sealed top of the inspection well inhibited the escape of explosive energy and significantly contributed to the maintenance of the explosion temperature in the inspection well. Conversely, the openings at both ends of the

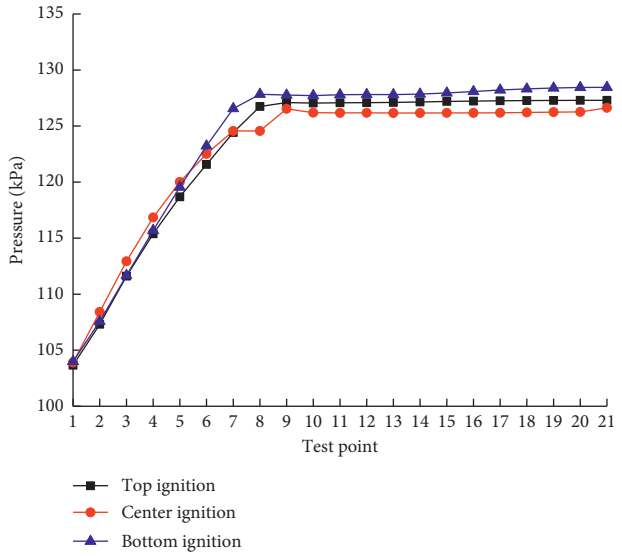

Figure 5: Curves of peak pressure under different ignition positions.

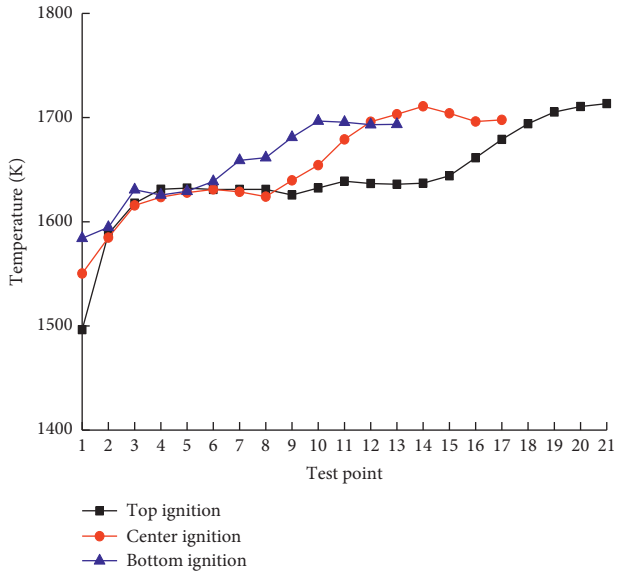

Figure 6: Curves of peak temperature under different ignition positions.

horizontal well promoted the escape of explosive energy. These simultaneous effects of "suppression" and "promotion" caused the peak explosion temperature to appear near the ignition point. The ability of the horizontal inspection well to inhibit the explosion energy through the dissipation effect was gradually reduced, and its ability to promote the explosion energy via the dissipation effect was gradually increased when the ignition positions were at the top, middle, and bottom of the inspection well. However, the dissipation effect of the inspection well upon the suppression of the explosion energy was still essential to maintaining the explosion temperature near the ignition point. Therefore, the peak value of the explosion temperature was gradually reduced, but the difference was not significant.

Furthermore, it can be seen from Figure 6 that with the development of the explosion process towards the left end of the horizontal well, the peak explosion temperatures decreased and reached their minimum at the left end of the horizontal well; the peak explosion temperatures were 1496 K, 1550 K, and 1584 K for the top, middle, and bottom ignition positions, respectively. Based on the analysis, as the distance between the test point and the left end of the horizontal well gradually decreased, the effect of the horizontal well on the dissipation of explosion energy gradually increased and had a significant role in influencing the explosion temperature. Therefore, the peak value of the temperature in the horizontal well gradually decreased, and the minimum value appeared at its left end.

3.1.3. Influence of the Ignition Position on the Flame Propagation Velocity. The area from the left end of the horizontal well to the ignition position was observed, and Figure 7 provides the flame propagation velocity variation curves for the various test points for the ignition positions at the top, middle, and bottom of the inspection well.

It can be seen from Figure 7 that when the ignition position was at the top of the inspection well, the flame propagation velocity increased with the distance to the ignition position (test points 21–13), except for near the corner of the inspection well (test points 13–11), where it decreased. It then increased towards the left end (test points 11–1). The variance in flame propagation velocities for the ignition positions at the middle of the inspection well was generally similar to that for the ignition at the top; near the corner of the inspection well (test points 13–11), it increased slightly at first and then decreased. Similarly, when the ignition position was at the bottom of the inspection well, the flame propagation velocity generally increased from the ignition position to the left end of the horizontal well (test points 13–11), increasing slightly at first and then decreasing near the corner of the inspection well (test points 13–11).

The analysis showed that the ignited flammable gases initially burned slowly with a low flame propagation velocity near the ignition position. Compared with the cases where the ignition positions were at the middle and bottom of the inspection well, when the ignition position was at the top, the inspection well underwent intense explosion and rapid flame propagation over a longer physical space, resulting in a significantly higher flame propagation velocity. In addition, the abrupt increase in the cross-sectional area resulted in obvious dilatancy as the flame spread from the bottom of the inspection well to the horizontal well (test points 13–11), thus causing the flame propagation velocity to decrease from 76.92 m/s to 53.33 m/s. Because there was less vertical distance between the ignition positions at the middle and bottom of the inspection well than that at the top, the velocity was relatively low after flame development. The dilatancy had little influence on the flame propagation velocity, which first increased slightly and then decreased from test point 13 to test point 11. For the middle and top

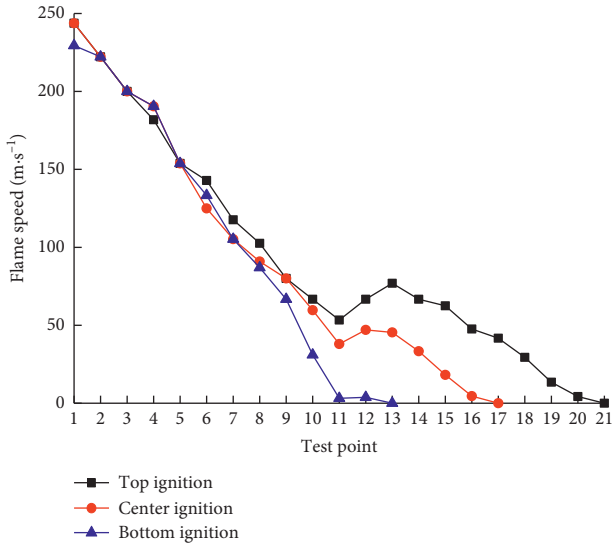

Figure 7: Curves of flame propagation velocity under different ignition positions.

ignition positions, the flame propagation velocities increased from 45.45 m/s and 0 m/s to 47.06 m/s and 3.79 m/s and then decreased to 38 m/s and 3.189 m/s, respectively.

Moreover, the direction of the explosion flame propagation changed abruptly from the vertical to the horizontal direction near the 90° corner junction between the inspection well and the horizontal well (test points 11–10). The higher turbulence intensity strengthened the component transport rate between the burned and unburned gases, leading to a higher flame propagation velocity. The flame shape rapidly elongated and generally developed from a "flat-straight shape" (Figures 8(a), 8(c), and 8(e)) to a "fingertip shape" (Figures 8(b), 8(d), and 8(f)). The explosion shock wave compressed the unburned gas in the horizontal well and pushed it forward, which generated turbulence, accelerated the combustion process, and caused the flame propagation velocity to increase gradually. The horizontal well was 20 m long on each side and open at both ends, which provided a semiopen space for the explosion flame development and accelerated the flame. The flame propagation velocity increased linearly along the direction to the left end of the horizontal well (test points 10–1) and peaked at the left end; the peak velocities were 243.75 m/s, 243.75 m/s, and 229.41 m/s when the ignition positions were at the top, middle, and bottom of the inspection well, respectively.

3.2. Influence of the Inspection Well Depth. As shown in Table 1, the inspection well depths were 2 m, 4 m, and 6 m, corresponding to test points 15, 17, and 16, respectively. The ignition position was at the middle of the inspection well, which was sealed at the top, and both ends of the horizontal well were open during the simulation. The inspection well and the horizontal well were filled with 6% CH_4.

3.2.1. Influence of the Inspection Well Depth on the Explosion Pressure. Test point 1 at the left end of the horizontal well, test point 6 at the middle of the horizontal well, test point 12 at the junction of the horizontal well and inspection well, and the test point at the middle of the inspection well (the ignition position) were observed. The pressure-time variation curves for various test points at inspection well depths of 2 m, 4 m, and 6 m, shown in Figure 9, were obtained from the simulation results.

Figure 9 shows that the pressure-time variation curves for various test points at the inspection well depths of 2 m, 4 m, and 6 m were similar, and all presented a trend of repeated increasing-decreasing oscillation. Due to the joint effects of the sealed top of the inspection well and the depressurisation effect at both ends of the horizontal well, the curves in Figure 9 demonstrated the same patterns of variation as those in Figure 4. With increasing distance from the ignition position (i.e., decreasing distance from the left port of the horizontal well), the pressure peak value and vibration amplitude gradually decreased. In contrast, the pressure oscillation maintained the fluctuation of the initial pressure. Furthermore, comparing Figures 9(a)–9(c) show that the peak pressure at these same test points (such as test point 12) also differed. The peak pressure variation curves at various test points for inspection well depths of 2 m, 4 m, and 6 m were obtained from the simulation results (Figure 10).

As shown in Figure 10, the peak pressure curves varied consistently for all inspection well depths, and all clearly demonstrated segmentation. However, the differences between the peak pressures significantly increased. In general, the peak pressure at a given test point grew at an increasing rate with increasing inspection well depth. During its stable stage, the peak pressure was maintained at approximately 124.6 kPa at the inspection well depth of 2 m and 126.3 kPa at the inspection well depth of 4 m (a 1.4% increase). For the 6 m well depth, the peak pressure remained at approximately 130.7 kPa, an increase of 4.9% and 3.5% as compared to those for depths of 2 m and 4 m, respectively. It was determined that for the middle ignition position, the physical space that caused the explosion pressure to rise within the relatively confined space increased with

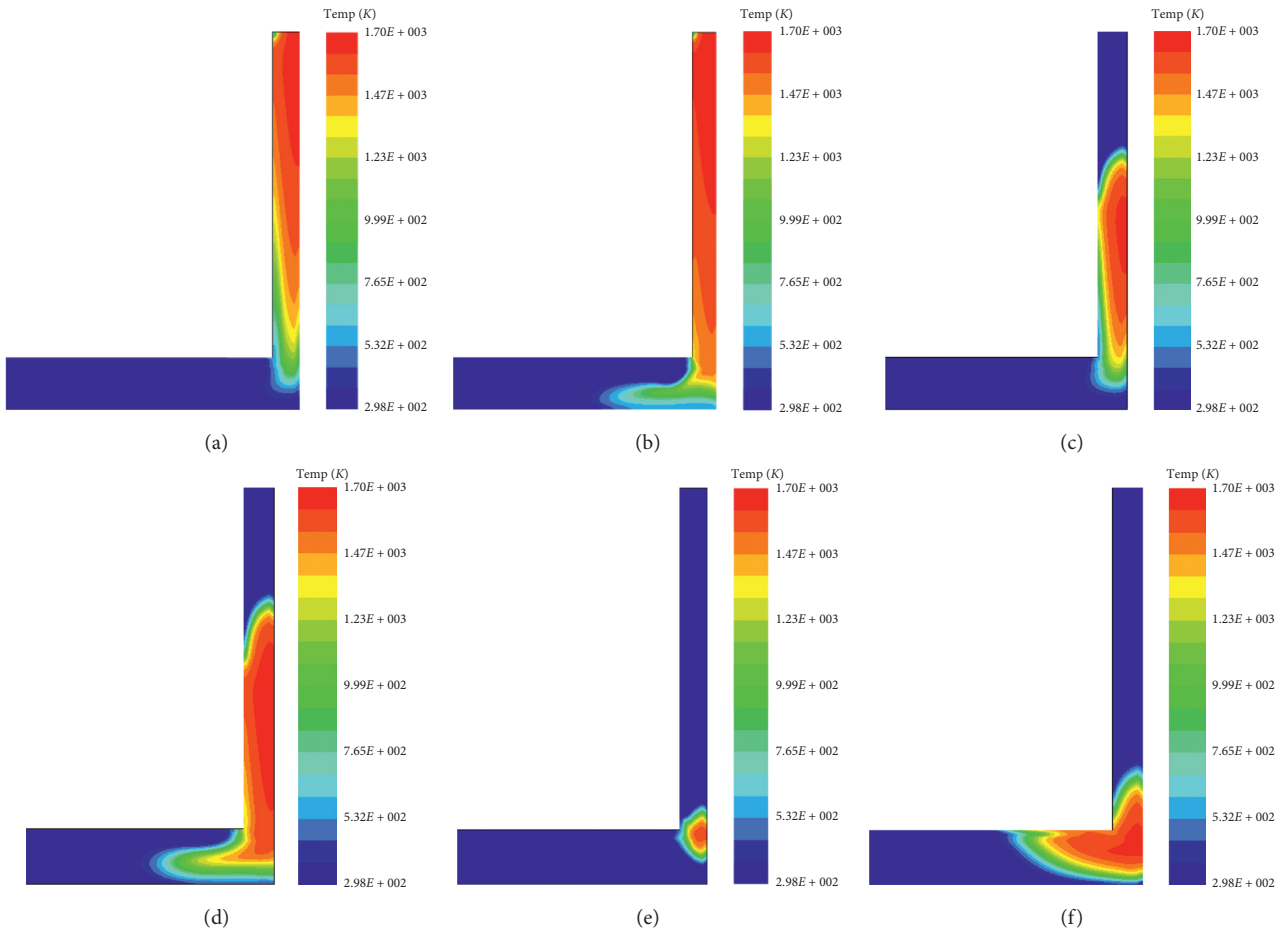

Figure 8: Flame propagation structure under different ignition positions: (a) top ignition 0.21 s; (b) top ignition 0.23 s; (c) center ignition 0.185 s; (d) center ignition 0.205 s; (e) bottom ignition 0.13 s; (f) bottom ignition 0.18 s.

inspection well depth due to its sealed top, thus promoting a strong chemical reaction. With a more intense explosion, there was higher overall peak pressure within the inspection well and the area of the horizontal well near the junction. Therefore, the peak pressure in the stable stage when the inspection well depth was 6 m was significantly higher than the values for 2 m and 4 m depths. It could thus be inferred that the peak pressure varies with the inspection well depth.

3.2.2. Influence of the Inspection Well Depth on the Explosion Temperature. The area from the left end of the horizontal well to the ignition position was observed for different inspection well depths. Figure 11 provides the peak explosion temperature variation curves at various test points for the 2 m, 4 m, and 6 m well depths.

Figure 11 shows that the peak temperature curves varied similarly to those in Figure 6. The peak temperatures near the ignition positions remained high and reached maximum values of 1701 K, 1710 K, and 1730 K for the 2 m, 4 m, and 6 m well depths, respectively, with a maximum increase of 1.7%. This was primarily due to the inspection well's sealed top, which inhibited the escape of the explosion energy and was substantially responsible for maintaining the explosion temperatures in the well. In the horizontal wells, as the explosion process proceeded towards the left end, the peak values of the explosion temperature gradually decreased, and the minimum values appeared at the end of the well primarily because the horizontal well promoted the dissipation of the explosion energy and significantly impacted the explosion temperature. The minimum temperatures were 1503 K, 1550 K, and 1515 K for the 2 m, 4 m, and 6 m well depths, respectively.

3.2.3. Influence of the Inspection Well Depth on the Flame Propagation Velocity. The area from the left end of the horizontal well to the ignition position was observed, resulting in flame propagation velocity variation curves for various test points at different inspection well depths, as shown in Figure 12.

The flame propagation velocity variation curves at the inspection well depths of 2 m, 4 m, and 6 m (Figure 12) were generally similar to those for the ignition positions at the top, middle, and bottom (Figure 7). The velocities peaked at the left end of the horizontal well (test point 1) and were 216.67 m/s, 243.75 m/s, and 243.75 m/s for the 2 m, 4 m, and 6 m well depths, respectively. In addition, the flame propagation was significantly accelerated as the inspection well depth increased, and it increased most quickly at the bottom

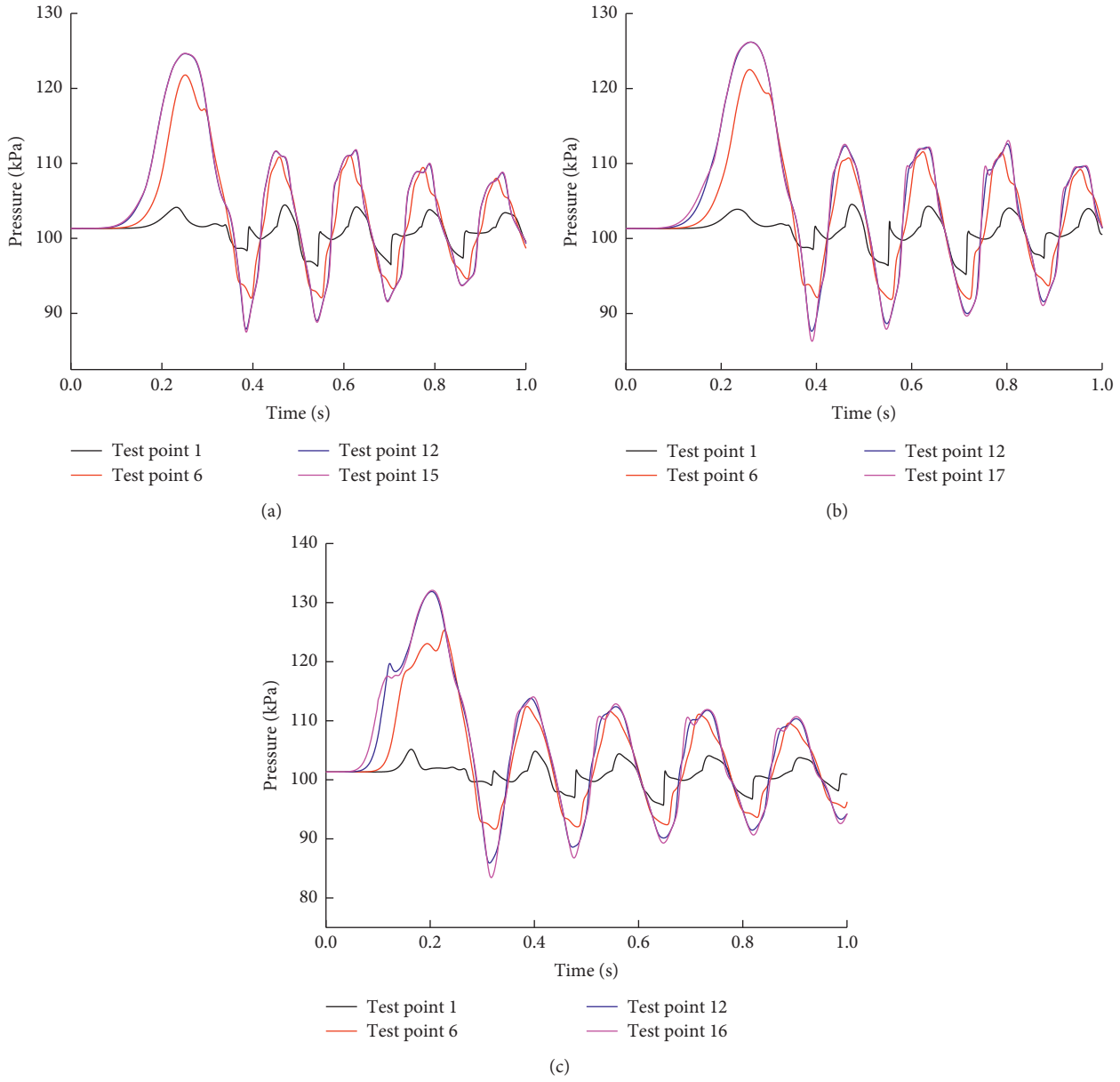

Figure 9: Curves of pressure vs. time under different inspection well depth: (a) 2 m; (b) 4 m; (c) 6 m.

of inspection well (test point 13). Specifically, the flame propagation velocity reached 105.26 m/s at the inspection well depth of 6 m, which was 21.57 times and 2.32 times those at the inspection well depths of 2 m and 4 m, respectively. Based on the analysis, after the combustible gas ignited in the inspection well, the flame developed slowly during the initial stage of reaction, and the propagation velocity near the ignition position was relatively low. Compared with the inspection well depths of 2 m and 4 m, the 6 m deep inspection well provided a longer physical space for the intensification of the explosion reaction and the quick development of the flame, resulting in the rapid increase in the flame propagation velocity.

3.3. Influence of the Gas Composition. Based on Table 1, which shows the simulation structure, inspection well depth, and ignition position, the corresponding positions were set to 4 m—the middle of the inspection well—and test point 17 to investigate the influences of different gas compositions on the explosion characteristics. The inspection well was sealed at the top, and both ends of the horizontal well were open during the simulation. The inspection well and the horizontal well were filled with 6% CH_4 for one test and 6% CH_4 + 1% C_8H_{18} for the other.

3.3.1. Influence of the Gas Composition on the Explosion Pressure. Test point 1 at the left end of the horizontal well, test point 6 at the middle of the horizontal well, test point 12 at the junction between the horizontal and inspection wells, and test point 17 at the middle of the inspection well were observed. The pressure-time variation curves shown in

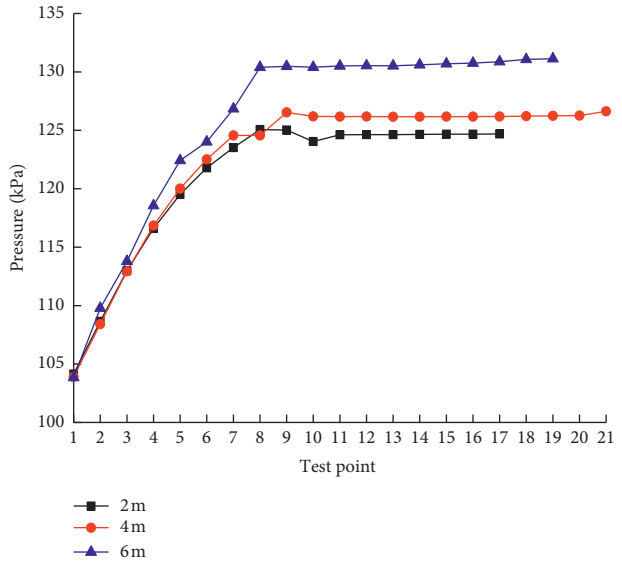

Figure 10: Curves of peak pressure under different inspection well depths.

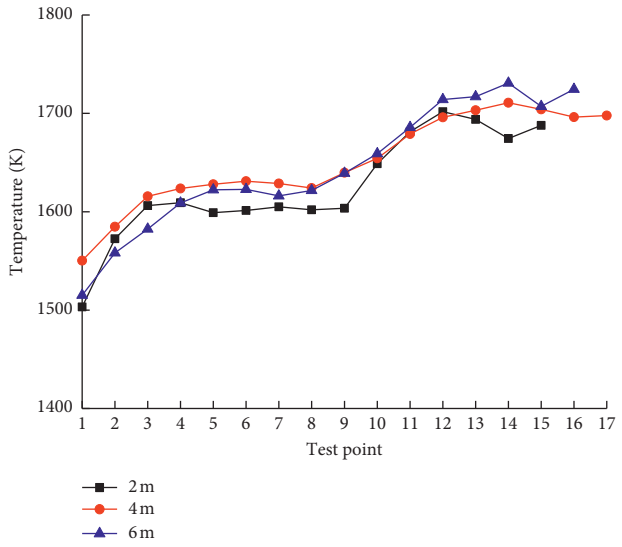

Figure 11: Curves of peak temperature under different inspection well depths.

Figure 13 were developed for the various test points for the 6% CH_4 and 6% CH_4 + 1% C_8H_{18} explosion reactions.

Figure 13 shows that the pressure-time variation curves for the 6% CH_4 and 6% CH_4 + 1% C_8H_{18} cases were similar to those in Figure 4, all of which demonstrated a trend of repeated increasing-decreasing oscillations. However, a comparison between Figures 13(a) and 13(b) indicates that the peak pressure at the same test points differed significantly in these two cases. Compared with the 6% CH_4, the time for the explosion of the 6% CH_4 + 1% C_8H_{18} to reach its peak pressure was reduced by 41.67%, from 0.24 s to 0.14 s. The peak pressure variation curves based on the simulation results for these two cases are shown in Figure 14.

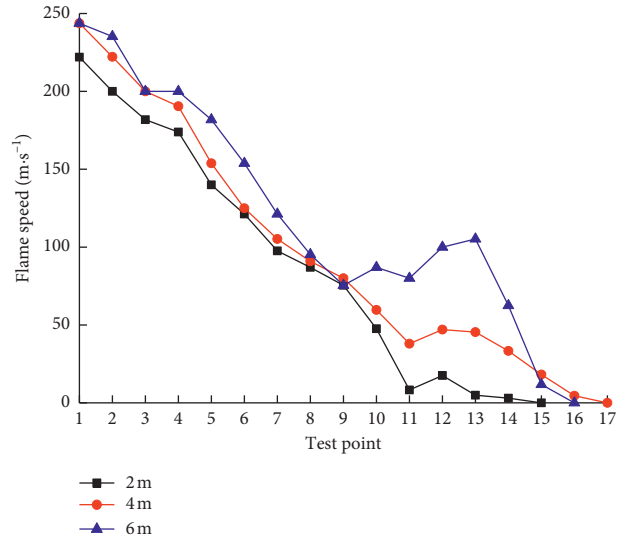

Figure 12: Curves of flame propagation velocity under different inspection well depths.

The peak pressure curves for the different gas compositions (Figure 14) were similar to those in Figure 5. These pressure curves were clearly segmented, but, for the same test points, the differences between the peak pressures of the different gas compositions increased dramatically. Specifically, for a given test point, the peak pressure generated by the explosion of the 6% CH_4 + 1% C_8H_{18} mixture was far higher than that by the 6% CH_4 explosion. In the stable pressure stage, the peak pressure generated by the explosion of 6% CH_4 + 1% C_8H_{18} and 6% CH_4 remained approximately at 340 kPa and 124.6 kPa, respectively; the former was 2.7 times of the latter. From test point 5 to test point 1, the peak pressure generated by the explosion of 6% CH_4 decreased, while that from the explosion of 6% CH_4 + 1% C_8H_{18} decreased after increasing. It was determined that the explosion of 6% CH_4 was in lean-burn, while that of 6% CH_4 + 1% C_8H_{18} was in rich-burn. There were more flammable gases involved in the explosion, for which the reaction was more intense, and the peak pressures at the various test points were also significantly higher than those generated from the explosion of 6% CH_4. Moreover, the explosion of 6% CH_4 + 1% C_8H_{18} changed from rich-burn to the state of chemical equivalent concentration or lean-burn due to the supplementation of fresh air near the left end of the horizontal well (test points 5–1) after venting. This further intensified the gas mixture reaction and, therefore, caused local pressure growth, indicating that different gas compositions can result in significant differences between the peak pressures.

3.3.2. Influence of the Gas Composition on the Explosion Temperature. The area from the left end of the horizontal well to the ignition position was observed, providing the peak temperature variation curves for the explosions of 6% CH_4 and 6% CH_4 + 1% C_8H_{18} at various test points (Figure 15).

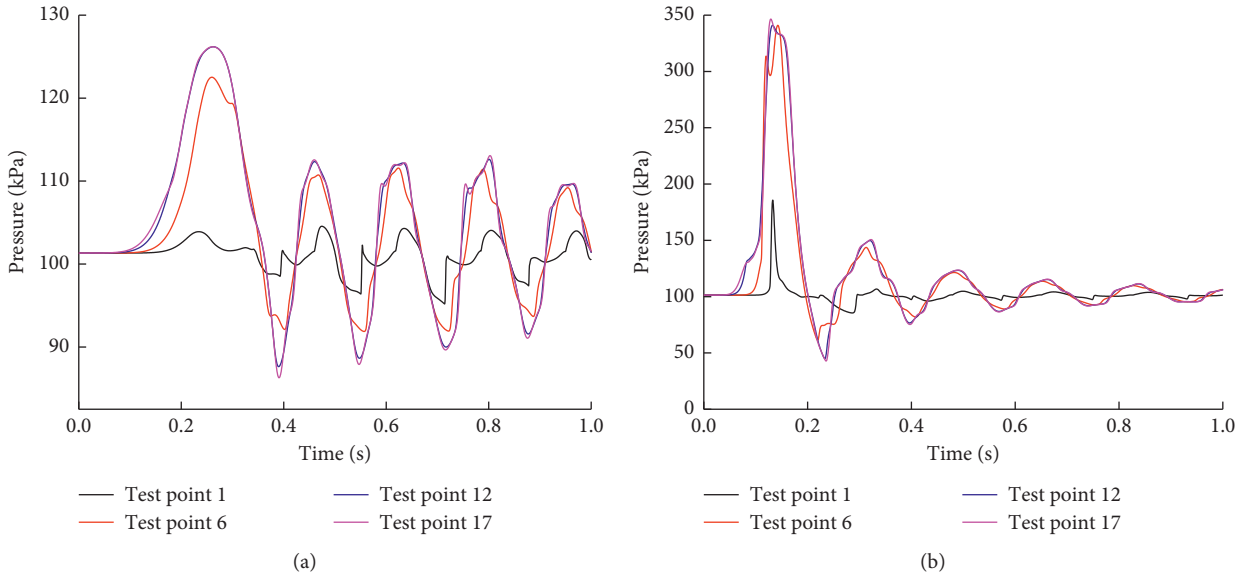

Figure 13: Curves of pressure vs. time under different gas compositions. (a) 6% CH_4. (b) 6% CH_4 + 1% C_8H_{18}.

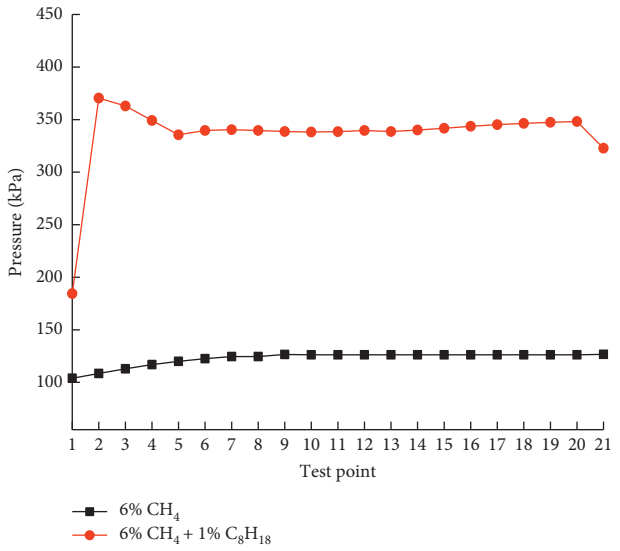

Figure 14: Curves of peak pressure under different gas compositions.

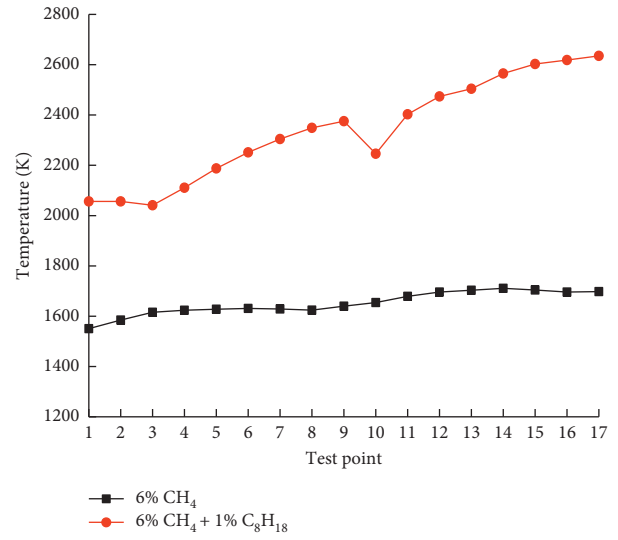

Figure 15: Curves of peak temperature under different gas compositions.

As shown in Figure 15, the peak temperature curves for the different gas compositions differed significantly from each other. The peak temperatures at the various test points during the explosions of 6% CH_4 + 1% C_8H_{18} in rich-burn far exceeded those of 6% CH_4 in lean-burn. Specifically, the peak temperature of the 6% CH_4 + 1% C_8H_{18} explosion was 2635 K near the ignition position, which was 1.54 times that of 6% CH_4. However, near the corner of the inspection well (test point 10), there was a sharp decrease in the peak temperature of the 6% CH_4 + 1% C_8H_{18} explosion, which was attributed to explosion temperature fluctuations resulting from the abrupt increase in the cross-sectional area at the corner. In addition, the two curves demonstrated opposite trends near the left end of the horizontal well (test points 3–1). The peak temperature of the 6% CH_4 + 1% C_8H_{18} explosion slightly increased because it changed from rich-burn to the state of chemical equivalent concentration or lean-burn due to the supplement of fresh air after the depressurisation from the end. Thus, the peak explosion temperature and its variation trend were significantly influenced by the gas composition.

3.3.3. Influence of the Gas Composition on the Flame Propagation Velocity. The area from the left end of the

horizontal well to the ignition position was observed; Figure 16 provides the flame propagation velocity variation curves at various test points for the explosion of 6% CH_4 and 6% CH_4 + 1% C_8H_{18}.

The flame propagation velocity curves of the two gas compositions displayed similar trends, as shown in Figure 16. With increasing distance to the ignition position, the flame propagation velocities first increased (test points 17–12), then decreased (test points 12–11), and then gradually increased again. The flame propagation velocity of the explosion of 6% CH_4 + 1% C_8H_{18} fluctuated within the horizontal well, but both peaked at the left end of the horizontal well (test point 1) with peak velocities of 243.75 m/s and 666.67 m/s, respectively; the latter was 2.74 times that of the former. For the same test points, the flame propagation velocities of the explosion of 6% CH_4 + 1% C_8H_{18} were higher than that of 6% CH_4, particularly in the horizontal well, where the flame propagation velocity of the former was approximately 610.12 m/s (2.5 times the peak value of the latter). It was observed that the 6% CH_4 + 1% C_8H_{18} explosion in rich-burn was more intense than that of 6% CH_4 in lean-burn, thus promoting rapid flame propagation. The flame propagation velocity fluctuated near the left end of the horizontal well due to the combined effects of the venting and supplementation of fresh air but remained high.

3.4. Influence of the Gas Concentration. As shown by the simulation structure in Table 1, the inspection well depth and ignition position were set to 4 m and the middle of the inspection well (corresponding to test point 17), respectively. The inspection well was sealed at the top, and both ends of the horizontal well were open during the simulation. Both the inspection well and the horizontal well were filled with C_8H_{18} at different concentrations (2%, 4%, and 6%).

3.4.1. Influence of the Gas Concentration on the Explosion Pressure. Test point 1 at the left end of the horizontal well, test point 6 at the middle of the horizontal well, test point 12 at the junction between the horizontal and inspection wells, and test point 17 at the middle of the inspection well were observed. Figure 17 provides the pressure-time variation curves for the various test points when the different concentrations (2%, 4%, and 6%) of C_8H_{18} exploded.

Figure 17 shows that the pressure-time variation curves for the various test points when the C_8H_{18} concentrations were 2%, 4%, and 6% were similar to those in Figure 4, all of which displayed a trend of repeated increasing-decreasing oscillations. With increasing C_8H_{18} concentrations, the peak pressures at the test points decreased gradually, and the times to attain the peak pressures, which were 0.22 s, 0.25 s, and 0.26 s, respectively, gradually increased. Compared with the 2% C_8H_{18} concentration, the times to reach the peak pressures with the 4% and 6% C_8H_{18} concentrations were 13.6% and 18.2% longer, respectively. The peak pressure variation curves resulting from the simulation are shown in Figure 18 for the various test points.

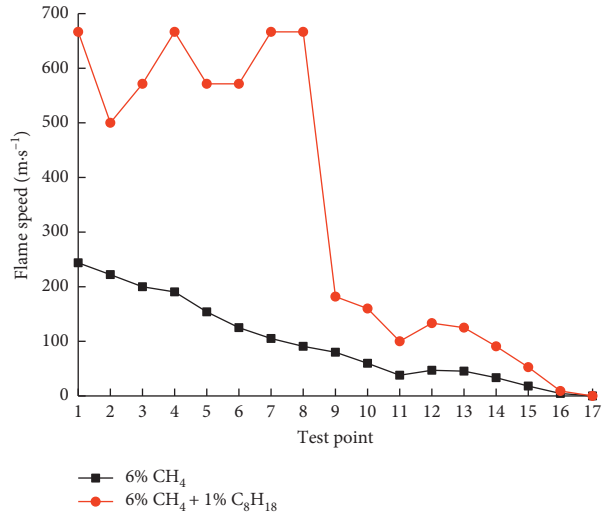

Figure 16: Curves of flame propagation velocity under different gas compositions.

As shown in Figure 18, the peak pressure curves displayed clear segmentation when the C_8H_{18} concentrations were 2%, 4%, and 6%, similar to the curves in Figure 5. However, there were significant differences in the peak pressures at the same test points; in general, the peak pressures decreased with increasing C_8H_{18} concentrations. In the stable pressure stage, the peak pressures were the highest; for the 2%, 4%, and 6% C_8H_{18} concentrations, the peak pressures were approximately 150 kPa, 136 kPa (a 9.3% decrease compared with the 2% case), and 132 kPa (a 12% decrease compared with the 2% case), respectively. It was determined that the C_8H_{18} explosion with an equivalent chemical concentration of 1.65% was in rich-burn for the 2%, 4%, and 6% concentrations. The incomplete mixture reaction intensified with increasing C_8H_{18} concentration, thus weakening the explosion intensity and reducing the peak explosion pressure. This indicated that peak pressure could vary significantly with different C_8H_{18} concentrations.

3.4.2. Influence of the Gas Concentration on the Explosion Temperature. The area from the left end of the horizontal well to the ignition position was observed. The peak explosion temperature variation curves for the 2%, 4%, and 6% C_8H_{18} concentrations are shown in Figure 19.

The peak temperature curves differed significantly at different gas concentrations, as shown in Figure 19. For a given test point, the peak temperature was the highest when the concentration of C_8H_{18} was 2%, followed by 4% and 6%. For the 2% concentration case, there was a peak (2353 K) on the peak curve that occurred near the ignition position. When the concentrations were 4% and 6%, there were double peaks on the peak curves near the left end of the horizontal well and the ignition position. The peak temperature for the 4% concentration was 2022 K; the two peaks remained equal. By comparison, the peak temperature for the 6% concentration was 1936 K, significantly higher than the peak temperature (1793 K) near the

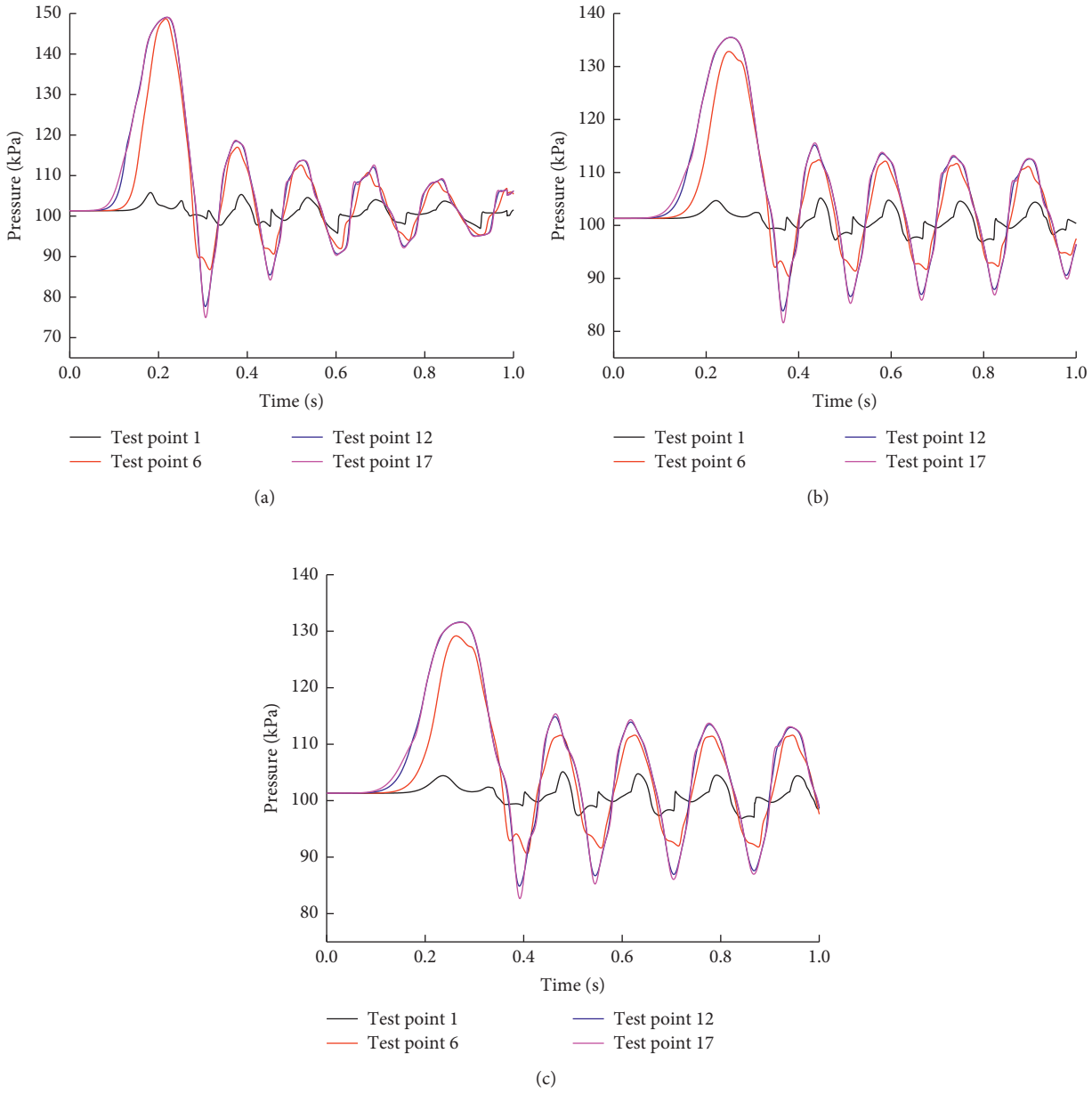

Figure 17: Curves of pressure vs. time under different gas concentrations: (a) 2% C_8H_{18}; (b) 4% C_8H_{18}; (c) 6% C_8H_{18}.

ignition position, and it occurred near the left end of the horizontal well. Compared with the case of the 2% C_8H_{18} concentration, when the C_8H_{18} concentrations were 4% and 6%, they significantly exceeded the chemical equivalent concentration of 1.65%. When the explosion wave spread to the left end of the horizontal well, an influx of fresh air mixed with the unburned C_8H_{18}. In the turbulence, the C_8H_{18} explosion further intensified, resulting in a significant temperature increase. These analyses indicated that the concentration of C_8H_{18} had a significant influence on the peak temperature.

3.4.3. Influence of the Gas Concentration on the Flame Propagation Velocity. The area from the left end of the horizontal well to the ignition position was observed. Figure 20 shows the flame propagation velocity variation curves for various test points at C_8H_{18} concentrations of 2%, 4%, and 6%.

The flame propagation velocity variation curves in Figure 20 reveal similar trends for the 2%, 4%, and 6% C_8H_{18} concentrations. With increasing distance to the ignition position, the flame propagation velocities first increased (test points 17–12), then decreased (test points 12–11), and gradually increased thereafter (test points 11–1). They peaked at 308 m/s, 267 m/s, and 250 m/s at the left end of the horizontal well for the 2%, 4%, and 6% C_8H_{18} concentrations, respectively. In addition, comparing the flame propagation velocities at the same test points suggested that they were the highest when the concentration of C_8H_{18} was

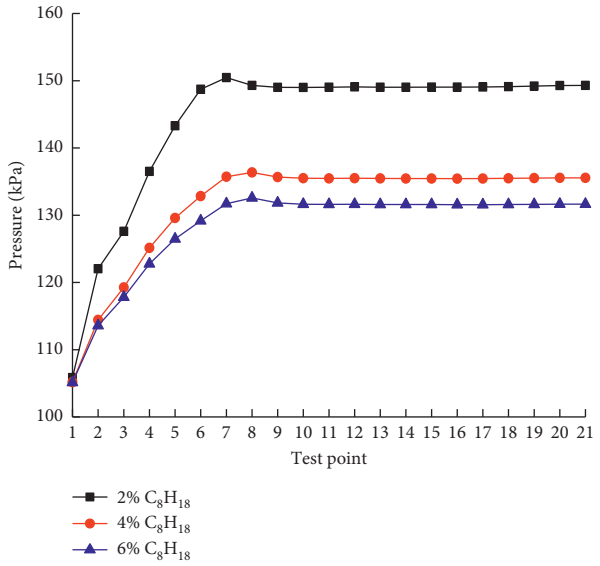

Figure 18: Curves of peak pressure under different gas concentrations.

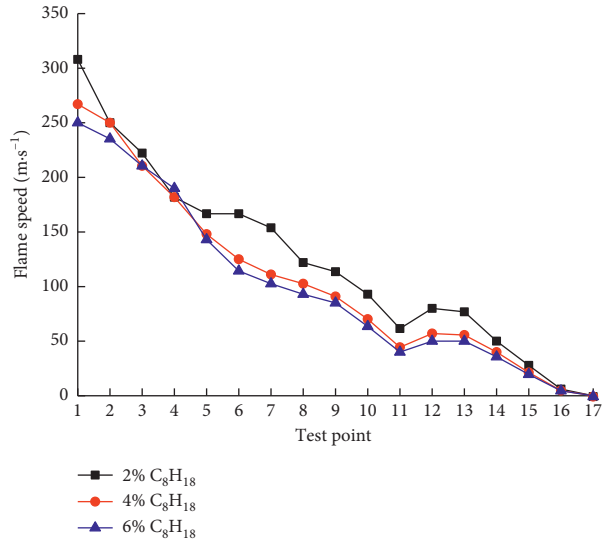

Figure 20: Curves of flame propagation velocity under different gas concentrations.

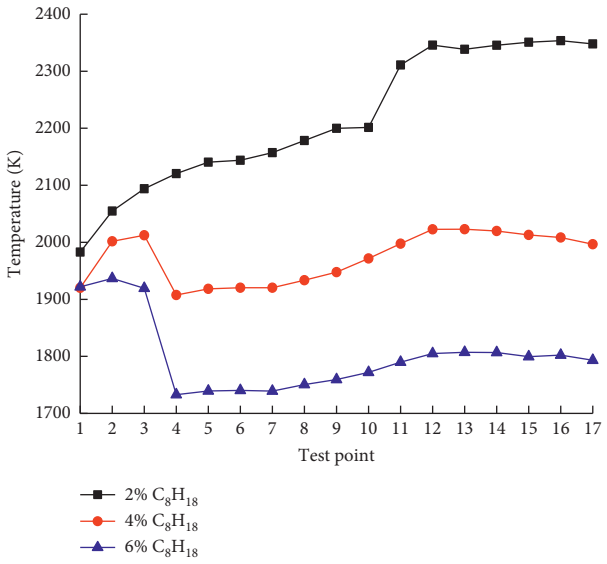

Figure 19: Curves of peak temperature under different gas concentrations.

2%, followed by 4% and 6%. According to the analysis, the C_8H_{18} explosion occurred under rich-burn conditions. The explosion intensities decreased with increasing concentrations, causing the flame propagation velocity to decrease continuously. Due to the length of the horizontal well and the venting at its left end, the flame accelerated, with the maximum flame propagation velocity occurring at the left end.

4. Conclusions

(1) This study investigated the influence of ignition position on explosion characteristics. For 6% CH_4 concentration and an inspection well depth of 4 m, the peak explosion pressures were 128 kPa, 127 kPa, and 129 kPa for the ignition positions at the top, middle, and bottom of the inspection well, respectively; the peak explosion temperatures were 1713 K, 1710 K, and 1705 K, respectively. Therefore, it can be concluded that the ignition position had little influence on the peak explosion pressure or temperature but significantly influenced the flame propagation velocity. In particular, near the junction between the inspection and horizontal wells, the flame propagation velocities differed significantly with the variations in the test conditions.

(2) The influence of the inspection well depth on the explosion characteristics was investigated. For a 6% CH_4 concentration, an ignition position at the middle of the inspection well, and inspection well depths of 2 m, 4 m, and 6 m, the peak explosion pressure ranged between 124.6 kPa and 130.7 kPa with a maximum increase of 4.9%; the peak explosion temperatures ranged between 1701 K and 1730 K with a maximum increase of 1.7%. This indicates that the inspection well depth had a minimal impact on the peak explosion pressure and temperature but significantly influenced the flame propagation velocity. Specifically, the flame propagation velocity peaked at the bottom of the inspection well with increasing inspection well depth.

(3) The influence of the gas composition on the explosion characteristics was analysed. When the ignition position was at the middle of the inspection well and the inspection well depth was 4 m, the peak explosion pressure, peak explosion temperature, and flame propagation velocity for the 6% concentration of $CH_4 + 1\%$ C_8H_{18} were significantly higher than those of 6% CH_4 alone. In the stable pressure stage,

the peak explosion pressure, peak explosion temperature, and maximum flame propagation velocity of the former were 2.7 times, 1.54 times, and 2.74 times those of the latter, respectively.

(4) The influence of the gas concentration on the explosion characteristics was also studied. For a 4 m inspection well depth, an ignition position at the middle of the inspection well, and 2%, 4%, and 6% C_8H_{18} concentrations, the peak explosion pressures were 150 kPa, 136 kPa, and 130 kPa, respectively; the peak explosion temperatures were 2353 K, 2022 K, and 1793 K, respectively; the peak flame propagation velocities were 308 m/s, 267 m/s, and 250 m/s, respectively. The peak explosion pressure, peak explosion temperature, and peak flame propagation velocity generally continued to decrease with increasing concentrations of C_8H_{18}.

Data Availability

The data used to support the findings of this study are available from the corresponding author upon request.

Conflicts of Interest

The authors declare that there are no conflicts of interest regarding the publication of this paper.

Acknowledgments

The authors thank the financial support of the National Nature Science Foundation of China (Grant No. 51604031), the Supporting Plan for the Construction of High-Level Teachers in Beijing Universities in 2019 (Grant No. CIT&TCD201904045), the Key Technology Project of Safety Production in 2017 of China (Grant No. Beijing-0007-2017AQ), Beijing University Student Scientific Research Training Project (2020), and the Beijing Natural Science Foundation Municipal Education Committee Joint Funding Project (Grant No. KZ201910017020). Meanwhile, the authors thank English translation service provided by Beijing T-norm Translation Service Co., Ltd, and thank Elsevier for retouching the revised version.

References

[1] G. Li, Y. Du, S. Qi, Y. Li, S. Wang, and B. Wang, "Explosions of gasoline-air mixtures in a closed pipe containing a T-shaped branch structure," *Journal of Loss Prevention in the Process Industries*, vol. 43, pp. 529–536, 2016.

[2] C. Wang, C. Guo, and S. Xu, "Experimental investigation on gaseous detonation propagation through a T-shape bifurcated tube," *Journal of Theoretical and Applied Mechanics*, vol. 36, no. 1, pp. 16–23, 2004.

[3] C. Zhai, B. Lin, Q. Ye, X. Li, and C. Zhu, "Influence of geometry shape on gas explosion propagation laws in bend roadways," *Procedia Earth and Planetary Science*, vol. 1, no. 1, pp. 193–198, 2009.

[4] R. Blanchard, D. Arndt, R. Grätz, M. Poli, and S. Scheider, "Explosions in closed pipes containing baffles and 90 degree bends," *Journal of Loss Prevention in the Process Industries*, vol. 23, no. 2, pp. 253–259, 2010.

[5] H. Xiao, X. He, Q. Wang, and J. Sun, "Experimental and numerical study of premixed flame propagation in a closed duct with a 90° curved section," *International Journal of Heat and Mass Transfer*, vol. 66, pp. 818–822, 2013.

[6] H. Xiao, J. Sun, and X. He, "A study on the dynamic behavior of premixed propane-air flames propagating in a curved combustion chamber," *Fuel*, vol. 228, pp. 342–348, 2018.

[7] Z. Yang, K. Zhou, and L. Xie, "Experimental study of flame transition in the *Z*-type tube," *Fire Safety Science*, vol. 15, no. 3, pp. 111–115, 2006.

[8] P. Zhang, Y. Du, Y. Zhou, S. Qi, S. Wu, and J. Xu, "Explosions of gasoline-air mixture in the tunnels containing branch configuration," *Journal of Loss Prevention in the Process Industries*, vol. 26, no. 6, pp. 1279–1284, 2013.

[9] L. Pang, J. C. Gao, Q. J. Ma et al., "Influence of bend structure on high-temperature flow after gas explosion," *Experimental Thermal and Fluid Science*, vol. 49, pp. 201–205, 2013.

[10] J. Chao, C. R. Bauwens, and S. B. Dorofeev, "An analysis of peak overpressures in vented gaseous explosions," *Proceedings of the Combustion Institute*, vol. 33, no. 2, pp. 2367–2374, 2011.

[11] J. Guo, X. Sun, S. Rui, Y. Cao, K. Hu, and C. Wang, "Effect of ignition position on vented hydrogen-air explosions," *International Journal of Hydrogen Energy*, vol. 40, no. 45, pp. 15780–15788, 2015.

[12] Z. Huang, Z. Liu, S. Chen, Y. Zhang, and Y. Zhang, "Numerical simulation and study on the transmission law of flame and pressure wave of pipeline gas explosion," *Safety Science*, vol. 50, no. 4, pp. 806–810, 2012.

[13] D. J. Park, Y. S. Lee, and A. R. Green, "Experiments on the effects of multiple obstacles in vented explosion chambers," *Journal of Hazardous Materials*, vol. 153, no. 1-2, pp. 340–350, 2008.

[14] A. R. Masri, S. S. Ibrahim, N. Nehzat, and A. R. Green, "Experimental study of premixed flame propagation over various solid obstructions," *Experimental Thermal and Fluid Science*, vol. 21, no. 1–3, pp. 109–116, 2000.

[15] D. Razus, C. Movileanu, V. Brinzea, and D. Oancea, "Closed vessel combustion of propylene-air mixtures in the presence of exhaust gas," *Fuel*, vol. 86, no. 12-13, pp. 1865–1872, 2007.

[16] B. Nie, X. He, R. Zhang, W. Chen, and J. Zhang, "The roles of foam ceramics in suppression of gas explosion overpressure and quenching of flame propagation," *Journal of Hazardous Materials*, vol. 192, no. 2, pp. 741–747, 2011.

[17] A. S. Huzayyin, H. A. Moneib, M. S. Shehatta, and A. M. A. Attia, "Laminar burning velocity and explosion index of LPG-air and propane-air mixtures," *Fuel*, vol. 87, no. 1, pp. 39–57, 2008.

[18] K. Sato, Y. Sakai, and M. Chiga, "Flame propagation along 90° bend in an open duct," *Symposium (International) on Combustion*, vol. 26, no. 1, pp. 931–937, 1996.

[19] M. Fairweather, G. Hargrave, S. Ibrahim, and D. Walker, "Studies of premixed flame propagation in explosion tubes," *Combustion and Flame*, vol. 116, no. 4, pp. 504–518, 1999.

[20] D. M. Valiev, V. y. Akkerman, M. Kuznetsov et al., "Influence of gas compression on flame acceleration in the early stage of burning in tubes," *Combustion and Flame*, vol. 160, no. 1, pp. 97–111, 2013.

[21] G. Thomas, G. Oakley, and R. Bambrey, "An experimental study of flame acceleration and deflagration to detonation transition in representative process piping," *Process Safety and Environmental Protection*, vol. 88, no. 2, pp. 75–90, 2010.

[22] L. Pang, T. Wang, Q. Zhang, Q. Ma, and L. Cheng, "Nonlinear distribution characteristics of flame regions from methane-air explosions in coal tunnels," *Process Safety and Environmental Protection*, vol. 92, no. 3, pp. 193–198, 2014.

[23] H. Hisken, G. A. Enstad, P. Middha, and K. van Wingerden, "Investigation of concentration effects on the flame acceleration in vented channels," *Journal of Loss Prevention in the Process Industries*, vol. 36, no. 1, pp. 447–459, 2015.

[24] S. Wan, M. Yu, K. Zheng, C. Wang, Z. Yuan, and X. Yang, "Effect of side vent size on a methane/air explosion in an end-vented duct containing an obstacle," *Experimental Thermal and Fluid Science*, vol. 101, pp. 141–150, 2019.